Supporting Information for

Rational Design of High-Performance Continuous-Flow Microreactors Based on Gold Nanoclusters and Graphene for Catalysis

Yanbiao Liu[a,c,d] , *Xiang Liu[a], Shengnan Yang[a], Fang Li[a,c], Chensi Shen[a,c], Manhong Huang[a,c], Junjing Li [d], Ricca Rahman Nasaruddin[b], Jianping Xie[b]**

[a] Textile Pollution Controlling Engineering Center of Ministry of Environmental Protection, College of Environmental Science and Engineering, Donghua University, 2999 North Renmin Road, Shanghai 201620, P. R. China. E-mail: yanbiaoliu@dhu.edu.cn; Fax: +86 21 6779 2522; Tel: +86 21 6779 8752.

[b] Department of Chemical and Biomolecular Engineering, National University of Singapore, 4 Engineering Drive 4, 117585 Singapore, E-mail: chexiej@nus.edu.sg; Fax: +65 6516 1936; Tel: +65 6516 1067.

[c] Shanghai Institute of Pollution Control and Ecological Security, 1239 Siping Road, Shanghai 200092, P. R. China.

[d] State Key Laboratory of Separation Membranes and Membrane Processes, Tianjin Polytechnic University, 399 Binshuixi Avenue, Tianjin 300387, P. R. China.

Supporting Information: 1 table and 14 figures.

Table S1. Characteristics of three real water samples.

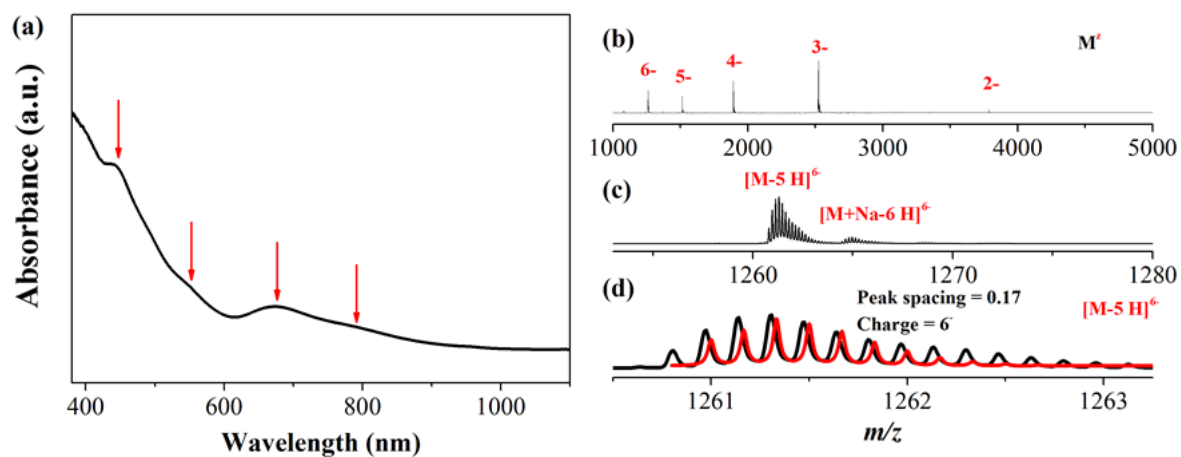| Real water sample	CODcr	pH	Conductivity	TDS
tap water	<25 mg/L	7.2	569.3　s/cm	287.4mg/L
surface water	84 mg/L	8.2	676.5　s/cm	337.1 mg/L
alkali-decrement wastewater (diluted by 1000 times before use)	37600 mg/L	13.6	90.36 ms/cm	45.0 g/L

Figure S1. (a) UV-vis absorption spectra and (b-d) ESI mass spectra of the as-synthesized $Au_{25}(MHA)_{18}$ clusters. M in (b-d) denotes $Au_{25}(MHA)_{18}$ and the red line in (d) is the simulated isotope pattern of $[Au_{25}(MHA)_{18} - 5H]^{6-}$.
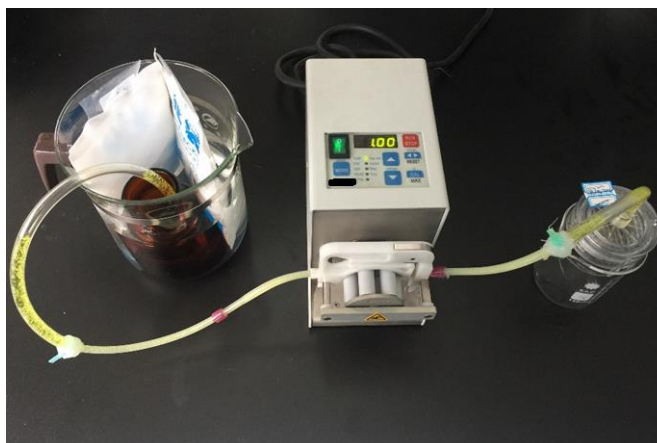
Figure S2. Experimental setup for the continuous flow catalytic reaction.

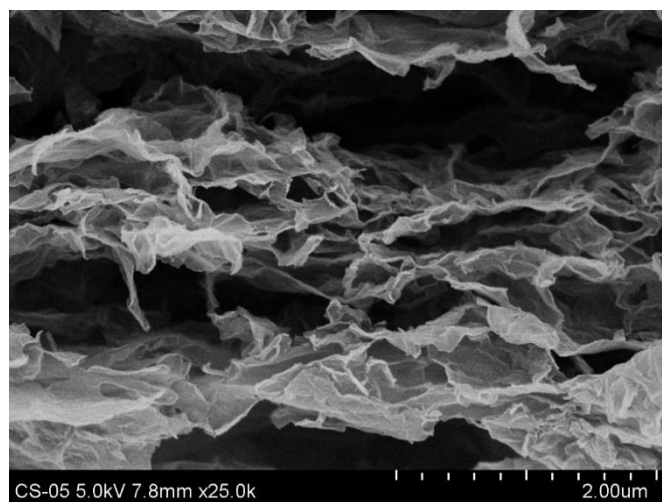**Figure S3.** FESEM image of cross-sectional analysis of the AuNC/4h-rGO catalytic membranes at high magnification, indicating the presence of nanochannels that are permeable to fluid.
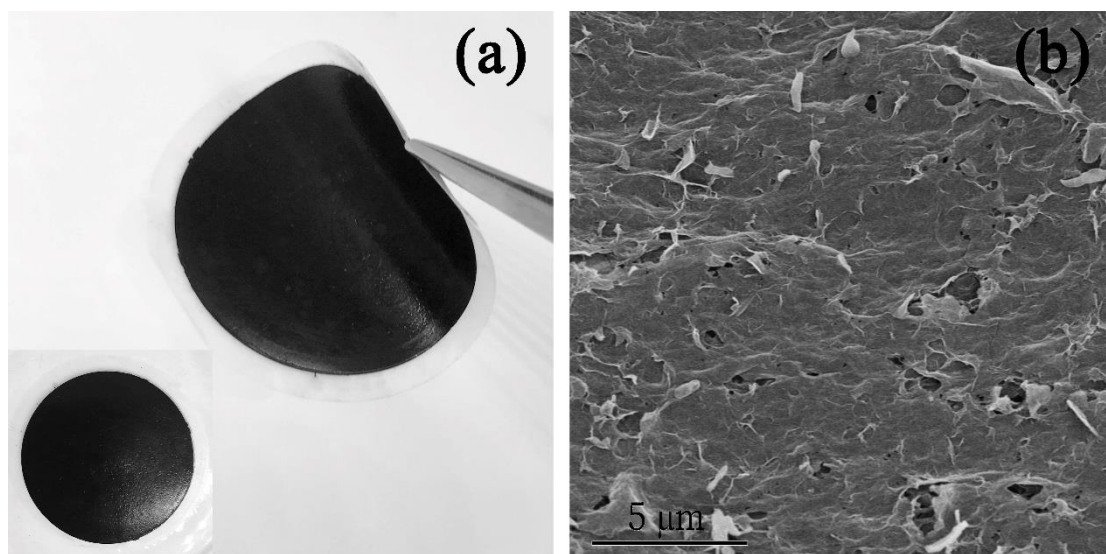
Figure S4. Photograph (a), FESEM image (b) of the AuNC/rGO membrane.
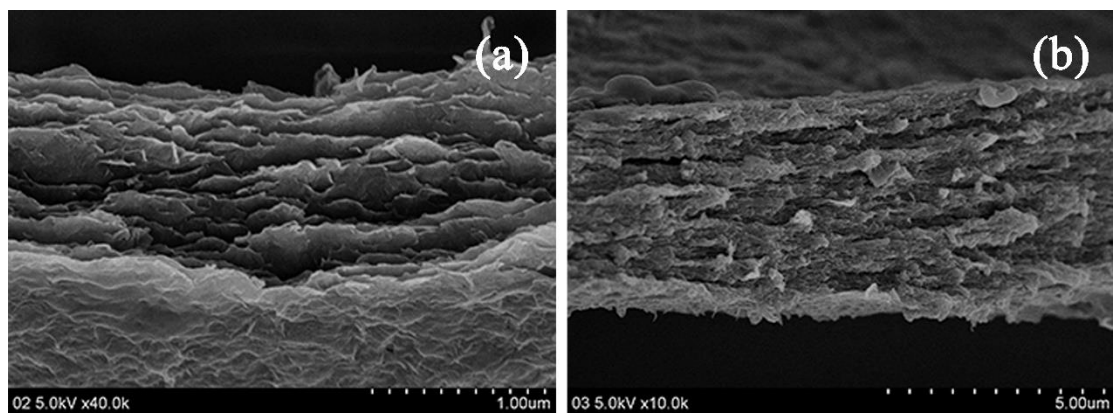
Figure S5. FESEM images for cross sectional analysis of the as-fabricated AuNC/4h-rGO hybrid catalytic membrane: 5 mg rGO (left) and 10 mg rGO (right).
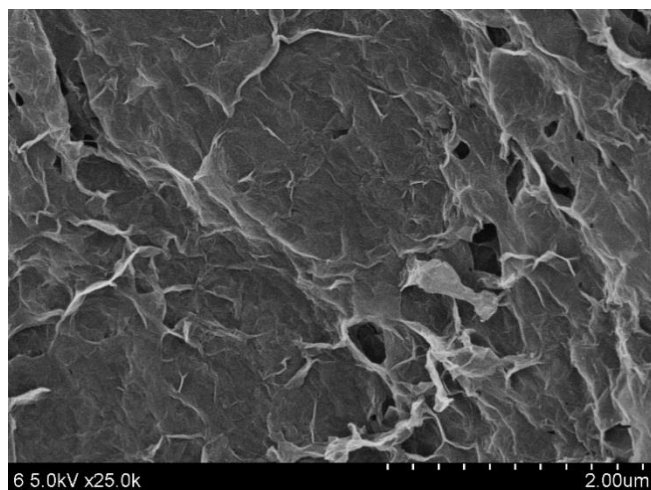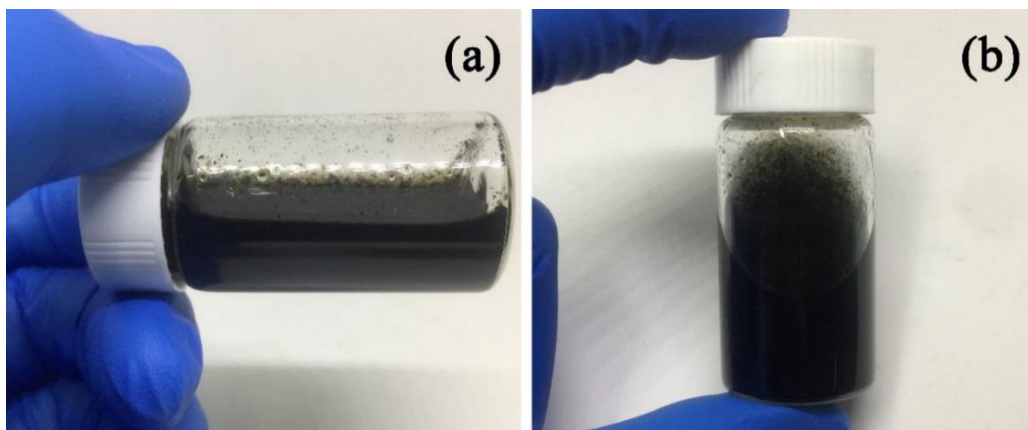
Figure S6. FESEM image of a typical rGO membrane.

Figure S7 (a) Digital picture of a 10h-rGO in DI-H_2O after 2 h continuous ultrasonication; (b) Digital picture of a 20h-rGO in AuNC solution after 2 h continuous ultrasonication.
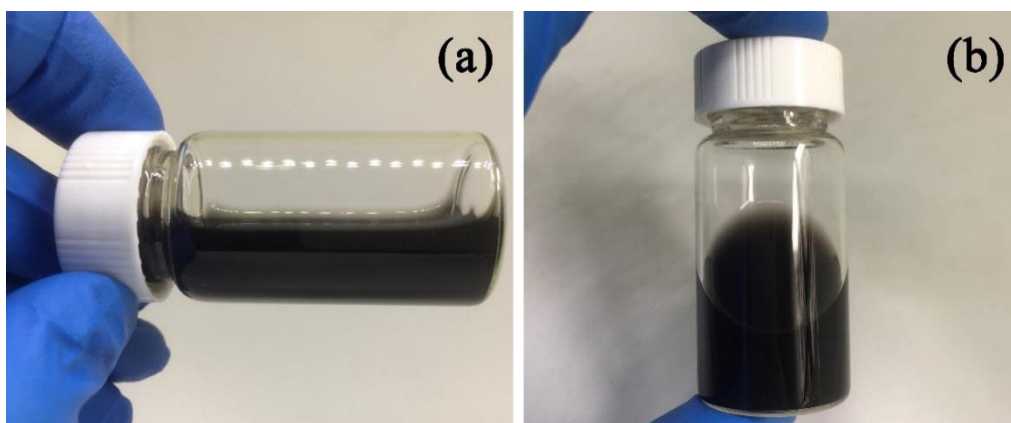
Figure S8. Digital picture of a 4h-rGO in AuNC solution after 20 min ultrasonication
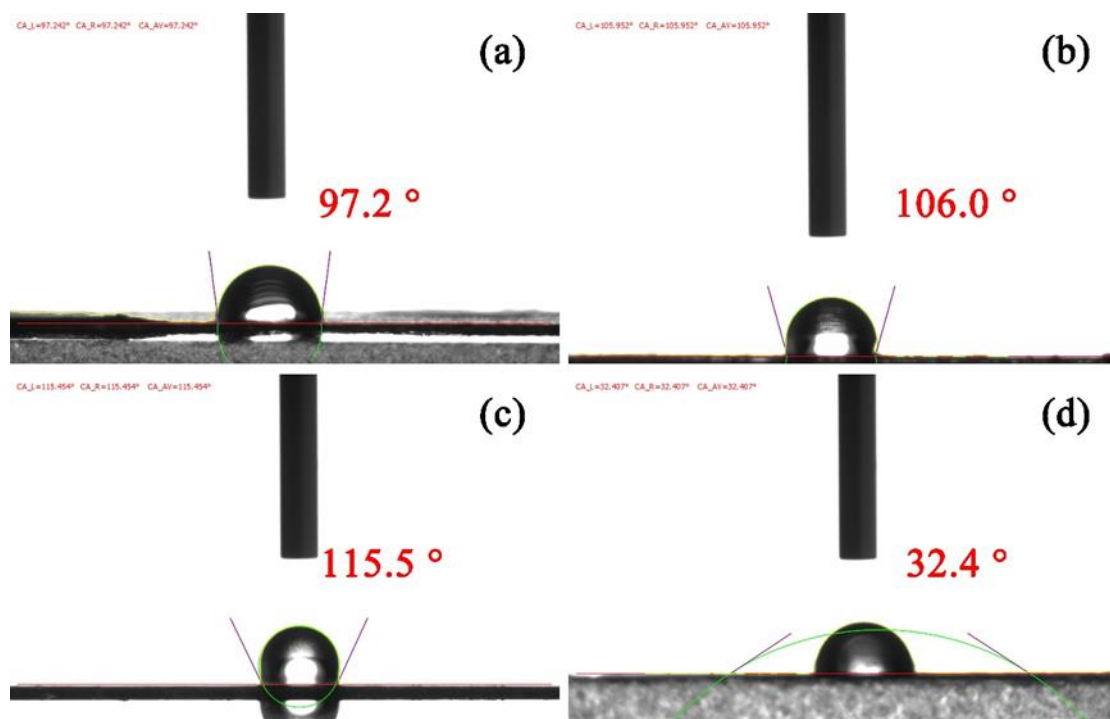
treatment.

Figure S9. Measurement of static contact angle of a water drop on rGO membrane surface with 4 h (a), 10 h (b), and 20 h (c) hydrothermal treatment. (d) The profile of a water drops on the AuNC/4h-rGO membrane (with 10 mol Au loading).
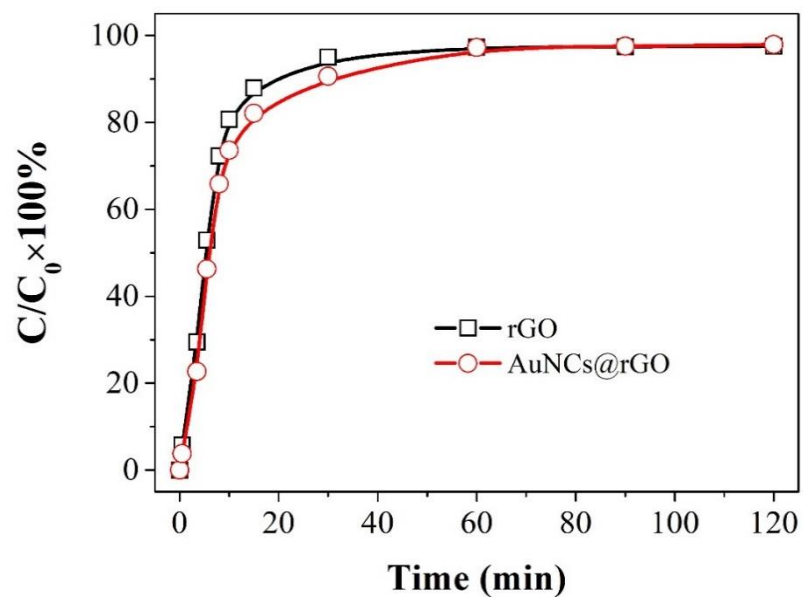
Figure S10. Breakthrough curves of rGO membrane and AuNC/4h-rGO membrane of
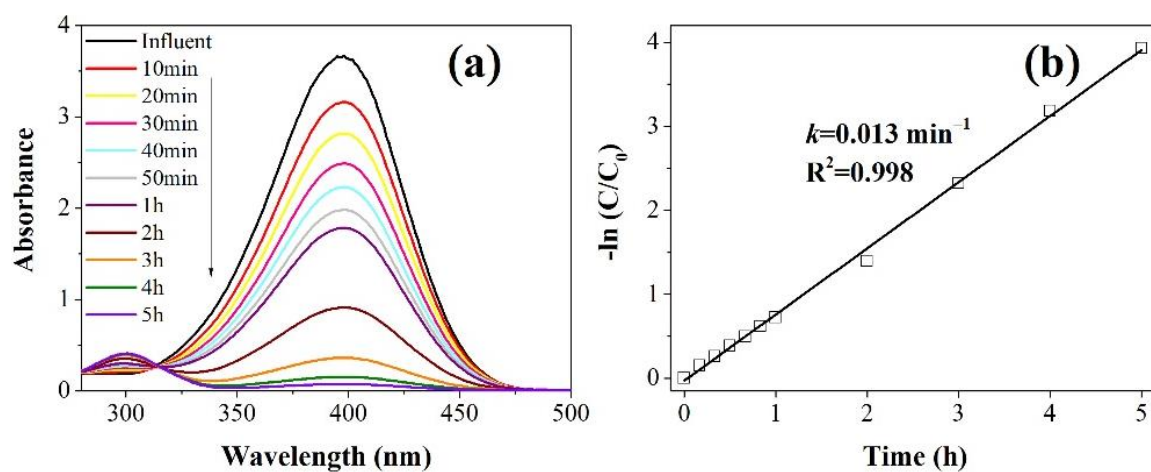
4-NP only.

Figure S11. (a) Time-dependent UV-vis adsorption spectra and (b) The reaction kinetics for the conversion of 4-NP in a batch reactor using AuNC/4h-rGO catalytic membrane.
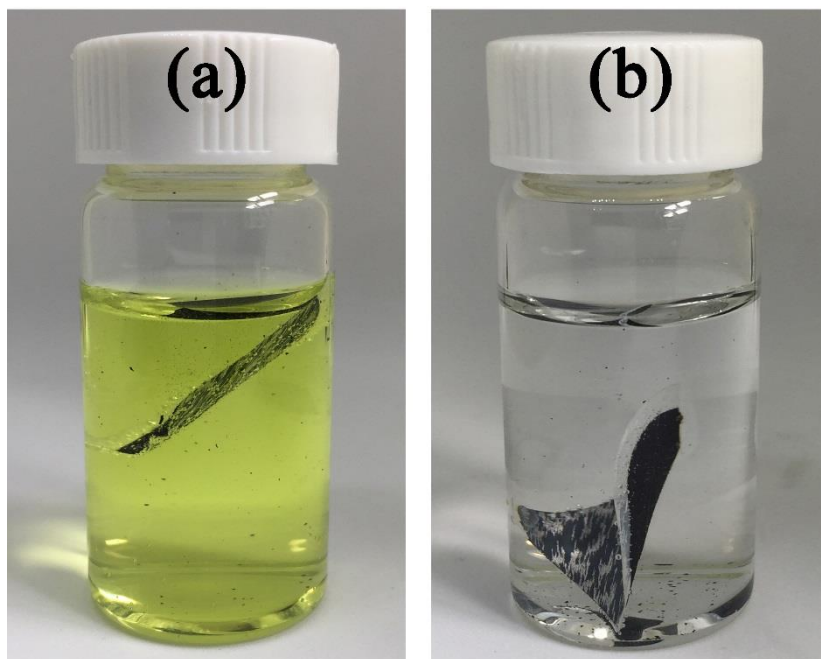
Figure S12. Digital photos of the batch reactor (a, at the beginning; b, after 5 h reaction)

towards the conversion of 4-nitrophenol using the AuNC/4h-rGO hybrid membrane.
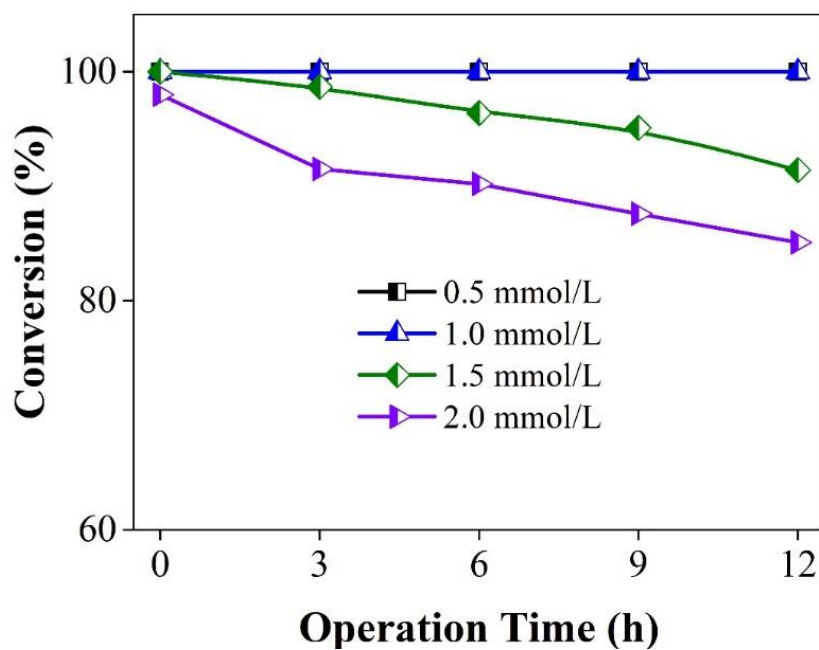
Figure S13. The effect of operation time and 4-NP concentration on the catalytic performance of an AuNC/4h-rGO membrane.
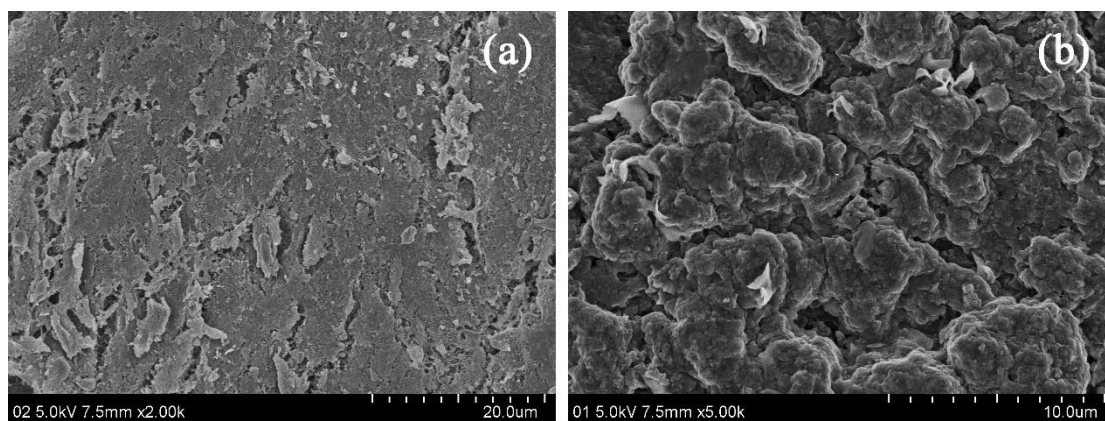
Figure S14. FESEM images of the AuNC/4h-rGO catalytic membrane after 12 h continuous operation (at different magnifications).